Imaging Density Disturbances in Water with a 41.3-Attosecond Time Resolution

P. Abbamonte,[1,*] K. D. Finkelstein,[2] M. D. Collins,[1] and S. M. Gruner[1,2]

[1]*Department of Physics, Cornell University, Ithaca, New York 14853-2501, USA*
[2]*Cornell High Energy Synchrotron Source, Cornell University, Ithaca, New York 14853-2501, USA*
(Received 15 November 2003; published 11 June 2004)

We show that the momentum flexibility of inelastic x-ray scattering may be exploited to invert its loss function, allowing real time imaging of density disturbances in a medium. We show the disturbance arising from a point source in liquid water, with a resolution of 41.3 attoseconds (4.13×10^{-17} s) and 1.27 Å (1.27×10^{-8} cm). This result is used to determine the structure of the electron cloud around a photoexcited chromophore in solution, as well as the wake generated in water by a 9 MeV gold ion. We draw an analogy with pump-probe techniques and suggest that energy-loss scattering may be applied more generally to the study of attosecond phenomena.

PACS numbers: 78.70.Ck, 87.64.Gb

Brisk progress has been made recently in the generation and detection of ultrashort, attosecond (1 as = 10^{-18} s) laser pulses with high harmonic generation techniques [1–8]. This has heralded an age of attophysics in which many-electron dynamics will be probed in real time. Much of what is already known about electron dynamics has been derived from energy-loss techniques such as inelastic x-ray, electron, or neutron scattering, which have been fruitfully applied to the study of, for example, plasma oscillations, exciton dynamics, and spin waves. Such experiments are normally examined in the frequency or momentum representation, where the spectra may be easily compared to theoretically calculable response functions for the electron density or local magnetic moment. However, if such measurements truly reflect dynamics, a temporal representation may also be illuminating.

In this Letter we demonstrate a method for inverting energy-loss measurements into time and space, permitting explicit imaging of electron dynamics in a medium. This allows the spatial extent of an excitation to be determined, i.e., its quantum dephasing distance, and a parallel with pump-probe techniques to be drawn. Inverting requires near complete energy and momentum parametrization of the loss function, so for its kinematic flexibility we consider the case of inelastic x-ray scattering (IXS).

In IXS a photon with well-defined initial momentum and energy, $(\mathbf{k}_i, \omega_i)$, is impinged on a specimen that scatters it to a final $(\mathbf{k}_f, \omega_f)$. The spectral density of scattered photons is proportional to the dynamic structure factor of the material, $S(\mathbf{k}, \omega)$, where $\omega = \omega_i - \omega_f$ and $\mathbf{k} = \mathbf{k}_i - \mathbf{k}_f$ are the transferred energy and momentum [9]. $S(\mathbf{k}, \omega)$ was posed originally by van Hove [10] as a measure of the dynamical properties of an interacting electron system, and by the fluctuation-dissipation theorem it is related to the imaginary part of a response function [11,12]

$$\mathrm{Im}[\chi(\mathbf{k}, \omega)] = -\pi[S(\mathbf{k}, \omega) - S(\mathbf{k}, -\omega)], \quad (1)$$

which can thereby be experimentally determined. $\chi(\mathbf{k}, \omega)$ is known as the density propagator and describes the way disturbances in the electron density travel about the system. $\chi(\mathbf{k}, \omega)$ is the space-time Fourier transform of $\chi(\mathbf{x}, t) = -i < 0|[\delta\hat{n}(\mathbf{x}, t), \delta\hat{n}(0, 0)]|0 > \theta(t)$, where $\delta\hat{n}$ is the density fluctuation operator, and in real space represents the disturbance produced by a delta function source at the origin at $t = 0$. Energy-loss scattering, in this sense, is rather like a pump-probe experiment; the system is perturbed at a reference point in time and its evolution observed. To make the analogy more concrete, we carry out an inversion on a real IXS data set.

Unfortunately, inverting requires knowledge of the full $\chi(\mathbf{k}, \omega)$, but experiment provides only its imaginary part. In other words, in IXS there is a phase problem that must be overcome before dynamics can be visualized explicitly. The phase in this case can be retrieved by exploiting the causal properties of $\chi(\mathbf{k}, \omega)$, i.e., the fact that it satisfies the second Kramers-Kronig (KK) relation [13]

$$\mathrm{Re}[\chi(\mathbf{k}, \omega)] = \frac{2}{\pi} P \int_0^\infty d\omega' \frac{\mathrm{Im}[\chi(\mathbf{k}, \omega)]}{\omega' - \omega}, \quad (2)$$

where P denotes the principal part. Equation (2) ensures that $\chi(\mathbf{x}, t) = 0$ for $t < 0$ and enforces retarded causality for the propagator. From (2) $\mathrm{Re}[\chi(\mathbf{k}, \omega)]$ may be determined, which, in principle, allows reconstruction of $\chi(\mathbf{x}, t)$ [14,15].

We used this procedure to image the disturbance generated by a point perturbation in liquid water. The elementary density quantum in water is the valence plasmon, which arises from collective vibration of the 2s and 2p shells of oxygen whose density determines the normal frequency $\omega_p = 22$ eV [16]. The plasmon is also the fundamental source of electronic screening in water and determines, for example, its optical refractive index [17]. We used IXS to sample its momentum and energy dependence on station C-1 at the Cornell High Energy Synchrotron Source (CHESS), where a nested Si(111)/(400) monochromator with sagittal focusing was used [18], and

at CMC-CAT at the Advanced Photon Source (APS), where a single Si(333) channel cut was used. Both experiments employed a diced, backscattering Ge(444) analyzer, fabricated by techniques described previously [19], to achieve overall energy and momentum resolutions of $\Delta\omega = 0.30$ eV and $\Delta k = 0.146$ Å^{-1}. At APS the plasmon count rate was 330 Hz at its peak, permitting 30 spectra to be taken over the momentum interval $0.476 < k < 4.95$ Å^{-1} in two days. The space and time resolutions are determined by the scan ranges to be $\Delta t = 2\pi\hbar/100$ eV $= 41.3$ as and $\Delta x = 2\pi/4.95$ Å$^{-1} = 1.27$ Å. The fields of view are determined by the resolutions to be $T = 13.8$ fs and $X = 54.3$ Å. Elastic scattering was fit and subtracted from the spectra, which were then extrapolated to 0 at $\omega = 0$, where Im$[\chi(\mathbf{k}, \omega)]$ must vanish by causality, and at $k = 0$, where it must vanish by charge conservation. The F sum rule was applied with $n_0 = 0.20$ Å^{-3} to set the absolute scale (Fig. 1).

While the proposed inversion procedure seems simple, unexpected subtleties arise when applying it to a discrete and finite data set. First, a discrete Im$[\chi(\omega)]$ implies that $\chi(t)$ is periodic, a property incompatible with the constraint that $\chi(t)$ vanish for all $t < 0$. Second, the KK relations are defined on an infinite ω interval, yet our scan range was a finite 100 eV. We resolve the former issue by analytically continuing the spectra onto a continuous freqency interval, by linear interpolation, resulting in a time axis that is formally infinite. $\chi(t)$ can then be evaluated with the time transform

$$\chi(t) = \int_0^\infty \frac{d\omega}{\pi} \, \sin(\omega t)\, \mathrm{Im}\chi(\omega) + \cos(\omega t)\, \mathrm{Re}\chi(\omega), \quad (3)$$

whose integrand oscillates rapidly but can be handled with standard numerical techniques. The $\chi(t)$ so obtained preserves causality, i.e., vanishes for all $t < 0$, but exhibits an aliasing effect that makes the dynamics repeat with a period $T = 13.8$ fs.

The latter issue is resolved by extrapolating the spectra to $\omega \to \infty$ with a Lorentzian fit, which is appended to the measured spectra (Fig. 2). This omits the influence of the $1s$ shell of oxygen, introducing a systematic error of order a few percent [20]. Extrapolating forces the time domain to be formally *continuous*, causing $\chi(\mathbf{x}, t)$ to be defined even on times much shorter than the effective resolution $\Delta t = 41.3$ as. It is fair to examine the function on such short time scales, though its behavior will be sensitive to the form of the extrapolation (Fig. 2). Once these steps are completed the spatial inversion $\chi(\mathbf{k}, t) \to \chi(\mathbf{x}, t)$ may be done with a standard spherical Fourier integral.

Figure 3 displays time frames of $\chi(\mathbf{x}, t)$ [21]. Because the medium is isotropic the disturbance is spherically symmetric, and each image is a section of this sphere with $\chi(\mathbf{x}, t)$ plotted in units of Å^{-6} on the vertical axis. At negative times $\chi(\mathbf{x}, t)$ vanishes and the system is "placid" [Fig. 3(a)]. At $t = 0$ the system is "struck" with a positive perturbation, generating a negative recoil at the origin
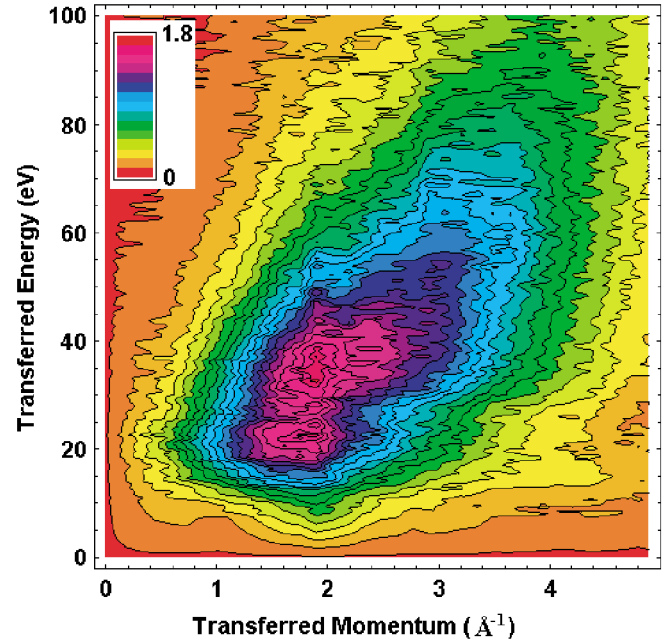

FIG. 1 (color). False color plot of $-\mathrm{Im}[\chi(\mathbf{k}, \omega)]$ for water in units of as/Å^3, plotted against transferred momentum (horizontal axis, in Å^{-1}) and energy (vertical axis, in eV). The broad feature is the valence plasmon, corresponding to collective oscillation of the $2s$ and $2p$ shells of oxygen.

surrounded by a positive buildup at $|x| = 1.3$ Å as current flows away from the source point [3(b)]. On an expanded scale a dip is also visible at $|x| = 2.5$ Å, followed by another peak at 3.8 Å [3(h)], forming a transient structure analogous to the Friedel oscillations that occur around point impurities in metals [22,23].
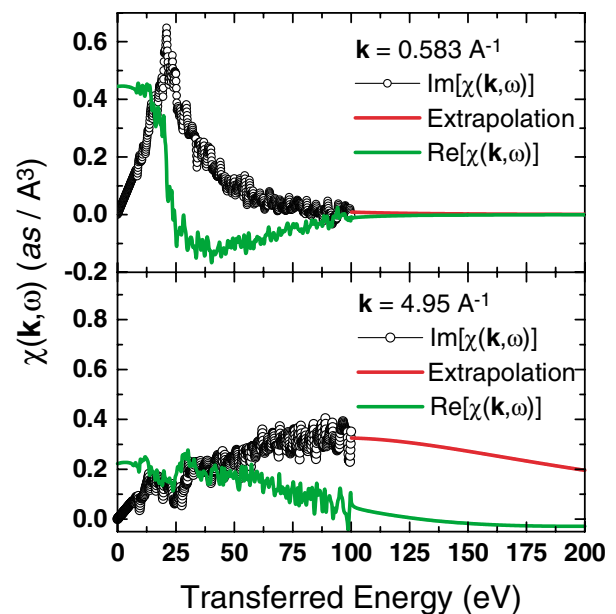

FIG. 2 (color). Individual spectra at $k = 0.583$ Å^{-1} (above) and $k = 4.95$ Å^{-1} (below), showing the raw data (open circles), extrapolated tails (red lines), and the resulting real part (green) line.
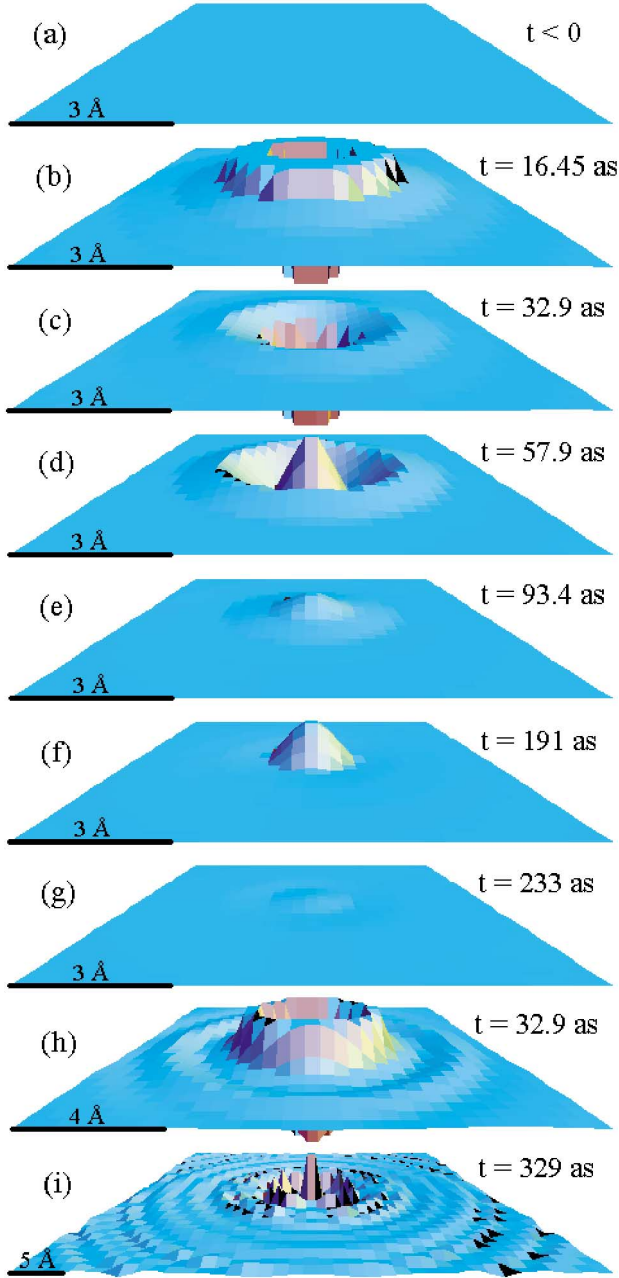
FIG. 3 (color). Time frames of $\chi(\mathbf{x}, t)$ derived from Fig. 1, in units of Å^{-6}. The vertical scale has been clipped at 1 Å^{-6} in frames (a)–(g), 0.1 Å^{-6} in (h), and 0.005 Å^{-6} in (i). Distances are indicated with scale bars. (a) At $t < 0$, before the perturbation, the system is "placid." (b) Shortly after the impulse, showing a large (off scale) negative recoil at $|x| = 0$ surrounded by compensating positive buildup. (c)–(g) Evolution of this disturbance at selected later times. (h) Same as (b) but on an expanded scale, showing distant Friedel-like oscillations. (i) After the disturbance has damped, scale expanded to show the experimental noise level.

Because of the compensating charge from the ion cores the pattern [3(h)] experiences a return force that causes it to reverse direction and change shape [3(c)]. An anharmonic oscillation occurs, with a time scale of order the plasma frequency $T = 2\pi/\omega_p = 180$ as [3(d)–3(g)].

Overall, the disturbance is seen to be rather local, occurring within 5 Å of the origin, a property related to the broad line shape in Fig. 1. A plasmon in water can oscillate a few times but never develops into a true propagating mode.

As time evolves the entropy grows and the disturbance damps as the system evolves toward thermal equilibrium. The disturbance decays below our threshold of detectability, shown by the experimental noise level in Fig. 3(i), after an elapsed time of 350 as—less time than it takes light to travel 100 nm in vacuum.

$\chi(\mathbf{x}, t)$ provides a means to visualize electron dynamics, but more significant is its relevance to a broad class of ultrafast processes in matter. Specifically, because it describes the disturbance from a point source, $\chi(\mathbf{x}, t)$ can be used through superposition to determine the effects of extended sources. The charge $n_{\text{ind}}(\mathbf{x}, t)$ induced in a medium by a time-dependent source $n_{\text{ext}}(\mathbf{x}, t)$ is determined in reciprocal space by the relationship [24]

$$n_{\text{ind}}(\mathbf{k}, \omega) = \frac{4\pi e^2}{\hbar k^2} \chi(\mathbf{k}, \omega) n_{\text{ext}}(\mathbf{k}, \omega), \qquad (4)$$

which in real space is a convolution over the dimensions of $n_{\text{ext}}(\mathbf{x}, t)$ identical to the Green's function integral used to handle sources in ordinary differential equations [25]. We illustrate its use by modeling an oscillating dipole and a gold ion traveling in water at 0.01 times the speed of light, c. As a model of the former, we take $n_{\text{ext}}(\mathbf{x}, t) = [\delta(x + 0.5 \text{ Å}) - \delta(x - 0.5 \text{ Å})]\cos(\omega_0 t)$, i.e., two charges with opposite sign separated by 1 Å, oscillating with a frequency $\omega_0 = 2$ eV$/\hbar$. The resulting disturbance, $n_{\text{ext}}(\mathbf{x}, t)$, shown in Fig. 4(a), occurs, for example, around a photoexcited chromophore in solution, and has influence on short-range fluorescence resonance energy transfer commonly used to measure distances in biological systems [26]. Similarly, an ion with charge Z traveling at velocity $\mathbf{v}$, represented as $n_{\text{ext}}(\mathbf{x}, t) = Z\delta(\mathbf{x} - \mathbf{v}t)$, for $Z = 79$ and $\mathbf{v} = 0.01c$ produces the pattern in Fig. 4(b). This is an image of the wake of a 9 MeV gold ion traveling in water and can be used, for example, to quantify the stopping power, dE/dx [27].
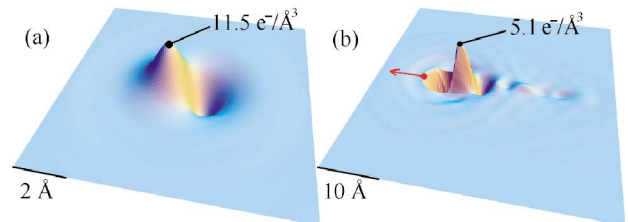

FIG. 4 (color). Electron density disturbances for two extended sources, constructed via Eq. (4). (a) Induced charge around an oscillating dipole, such as a photoexcited chromophore in solution, at the peak of its cycle and (b) the wake produced in water by a 9 MeV gold ion. The ion location and direction of motion are indicated by the red arrow.

It is important to address the issue of why, despite the spatial resolution of $dx = 1.27$ Å, individual atoms are not visible in Figs. 3 and 4. A density propagator is actually a function of two spatial variables, $\chi(\mathbf{x}, \mathbf{x}'; t)$, with a Fourier transform of the form $\chi(\mathbf{k}, \mathbf{k}'; \omega)$. With only one momentum transfer in scattering, we measure only the diagonal (i.e., longitudinal) response, $\chi(\mathbf{k}, \mathbf{k}; \omega)$ [11]. So the present analysis has assumed a translational invariance that does not strictly apply. The images in Figs. 3 and 4 must therefore be thought of as spatial averages—not single events, but the mean of many events at different locations in the specimen. This limitation in principle can be overcome by using standing wave techniques [28,29].

The existence of nonlocality in electrodynamics, in both time and space, is well established [13,30]. Here we have shown that they may be combined to explicitly image electron dynamics. Because x rays are tunable over broad ranges of energy, time scales are accessible that are currently out of the reach of laser-based techniques. We therefore suggest that IXS may provide an alternative window on the attosecond phenomena targeted in Refs. [1–8]. A sensible starting point for comparison would be the photofragmentation reaction of NaI or LiF.

Not all attosecond phenomena may be probed with IXS. Like x-ray diffraction, it is sensitive only to phenomena that modulate the electron density, that is, that are capable of screening charge, such as collective modes like plasmons and phonons. This makes IXS somewhat inappropriate for the study of low energy single particle excitations except in materials that cannot sustain collective electronic vibration, such as large gap insulators [31]. On the other hand, low energy electronic screening, which is determined by the plasmon through its real part, is quite accessible.

*Present address: Building 725D, Brookhaven National Laboratory, Upton, NY 11973, USA.

[1] M. Drescher et al., Science 291, 1923 (2001).

[2] M. Drescher et al., Nature (London) 419, 803 (2002).

[3] A. Baltuska et al., Nature (London) 421, 611 (2003).

[4] M. Hentschel et al., Nature (London) 414, 509 (2001).

[5] R. Kienberger et al., Science 297, 1144 (2002).

[6] H. Niikura, F. Légaré, R. Hasbani, M. Y. Ivanov, D. M. Villeneuve, and P. B. Corkum, Nature (London) 421, 826 (2003).

[7] H. Niikura, F. Légaré, R. Hasbani, M. Y. Ivanov, D. M. Villeneuve, and P. B. Corkum, Nature (London) 417, 917 (2002).

[8] P. M. Paul et al., Science 292, 1689 (2001).

[9] W. Schülke, in Handbook on Synchrotron Radiation, edited by D. E. Moncton and G. Brown (North-Holland, Amsterdam, 1991), Vol. 3, p. 565.

[10] L. van Hove, Phys. Rev. 95, 249 (1954).

[11] K. Sturm, Z. Naturforsch. 48a, 233 (1993).

[12] P. M. Platzman and P. A. Wolff, Waves and Interactions in Solid State Plasmas (Academic Press, New York and London, 1973).

[13] J. D. Jackson, Classical Electrodynamics (John Wiley & Sons, New York, 1975), 2nd ed., Chap. 7.10.

[14] There are cases, such as near a charge density wave instability, in which the Kramers-Kronig relations are violated at nonzero momentum transfer. See P. Martin, Phys. Rev. 161, 143 (1967).

[15] There is a trick in some cases for circumventing the KK transform. See V. A. Madsen and G. R. Satchler, Phys. Rev. C 48, 1221 (1993).

[16] H. Hayashi, N. Watanabe, Y. Udagawa, and C.-C. Kao, Proc. Natl. Acad. Sci. U.S.A. 97, 6264 (2000).

[17] $\chi(\mathbf{k}, \omega)$ is related to the refractive index by $n^2(\mathbf{k}, \omega) = 1 - (4\pi e^2/\hbar k^2)\chi(\mathbf{k}, \omega)$. At $\omega = 2$ eV as $k \to 0$ our data converge to $n = 1.37$, close to the correct value $n = 1.33$.

[18] K. D. Finkelstein, P. Abbamonte, and V. O. Kostroun, Proc. SPIE Int. Soc. Opt. Eng. 4783, 139 (2002).

[19] P. Abbamonte, Ph.D. thesis, University of Illinois, Urbana, Illinois, 1999.

[20] E. Shiles, T. Sasaki, M. Inokuti, and D. Y. Smith, Phys. Rev. B 22, 1612 (1980).

[21] See EPAPS Document No. E-PRLTAO-92-022422 for time series images of the density propagator. A direct link to this document may be found in the online article's HTML reference section. The document may also be reached via the EPAPS homepage (http://www.aip.org/pubservs/epaps.html) or from ftp.aip.org in the directory /epaps/. See the EPAPS homepage for more information.

[22] J. Friedel, Philos. Mag. 43, 153 (1952).

[23] These oscillations arise from the $\mathbf{k}$ dependence of $\chi(\mathbf{k}, \omega)$ in the same way that Friedel oscillations arise from the static susceptibility, $\chi(\mathbf{k})$. Because they involve highly excited states, they do not necessarily occur at a nesting vector, $2k_F$.

[24] D. Pines, Elementary Excitations in Solids (Addison-Wesley, Reading, MA, 1963).

[25] J. Mathews and R. L. Walker, Mathematical Methods of Physics (W. A. Benjamin, Inc., New York, NY, 1964).

[26] L. Stryer and R. P. Haugland, Proc. Natl. Acad. Sci. U.S.A. 58, 719 (1967).

[27] D. R. Penn, Phys. Rev. B 35, 482 (1987).

[28] W. Schülke, Phys. Lett. A 83, 451 (1981).

[29] J. A. Golovchenko et al., Phys. Rev. Lett. 46, 1454 (1981).

[30] V. M. Agranovich and V. L. Ginzburg, Spatial Dispersion in Crystal Optics and the Theory of Excitons (John Wiley & Sons, London, 1966).

[31] W. A. Caliebe, J. A. Soininen, E. L. Shirley, C.-C. Kao, and K. Hämäläinen, Phys. Rev. Lett. 84, 3907 (2000).